

# Cobalt-Doping-Induced Synthesis of Ceria Nanodisks and Their Significantly Enhanced Catalytic Activity

Xiao-Hui Guo,\* Chao-Chao Mao, Ji Zhang, Jun Huang, Wa-Nv Wang, Yong-Hui Deng, Yao-Yu Wang, Yong Cao, Wei-Xin Huang, and Shu-Hong Yu\*

Dimension- and shape-tunable nanoarchitectures have attracted rapidly growing interest due to their structure-dependent properties and important technological applications in the past few decades.<sup>[1,2]</sup> The manipulation of nanomaterials with specific structures possessing exceptional physics and chemical properties, via conveniently modulating the synthetic conditions, is one of the challenging issues in materials science.<sup>[3]</sup> Recently, much attention has been paid to shape- and size-controlled synthesis of metal oxide nanostructures (e.g., rare earth compounds<sup>[4]</sup> and transition metal oxides<sup>[5]</sup>) with unique performances.

As an important rare earth oxide, ceria ( $\text{CeO}_2$ ) has attracted considerable attention due to its extensive applications in catalysts, three-way catalysts (TWCs), solid oxide fuel cells, gates for metal-oxide semiconductor devices, biosensors, and phosphors.<sup>[6–8]</sup> In addition, it is abundant and has minimal toxicity and low cost, which makes it suitable for optoelectronic and photocatalytic applications.<sup>[9]</sup> Meanwhile, much effort has also been devoted to developing new synthetic methodologies for controlled synthesis of  $\text{CeO}_2$  nanocrystals, such as thermal decomposition,<sup>[10]</sup> flash combustion,<sup>[11]</sup> mechanochemical processing,<sup>[12]</sup> homogeneous precipitation,<sup>[13]</sup> electrochemical synthesis,<sup>[14]</sup> and hydrothermal<sup>[15]</sup>

and solvothermal processes.<sup>[16]</sup> More recently, Inoue et al. prepared ultrafine 2 nm ceria nanoparticles (NPs) by oxidation of cerium metal under solvothermal conditions.<sup>[17]</sup> Yan et al.<sup>[10]</sup> synthesized highly dispersible polyhedron-like ceria NPs via thermolysis of benzoylacetate complex precursors in oleic acid/oleylamine solvents. In particular, colloidal cubic  $\text{CeO}_2$  particles can be obtained via a simple green chemistry approach.<sup>[18]</sup> Uniform spherical, wire, and tadpole-shaped ceria nanostructures have been synthesized by a nonhydrolytic sol-gel process.<sup>[19]</sup> However, a unique two-dimensional (2D) flakelike ceria nanostructure has been rarely reported. Usually, the single-crystalline ceria nanosheets synthesized in the aqueous phase turned out to be of low quality and low yield,<sup>[20]</sup> which may limit their further applications.

It is well known that many applications of ceria NPs arise from the low-temperature redox potential between the  $\text{Ce}^{3+}$  and  $\text{Ce}^{4+}$  states and the high mobility of oxygen vacancies in the nanoscale regime. Upon reduction of the size of ceria particles, the lattice constant and  $\text{Ce}^{3+}$  concentration increases accordingly.<sup>[21]</sup> To maintain the charge neutrality, oxygen vacancies could be created, which increases oxygen diffusion and thereby increases the ease with which the material can absorb and release oxygen. Besides, recent work has demonstrated that selective doping can improve the electron-transfer or redox properties of bulk ceria, which can significantly reduce the grain boundary resistance and the activation energy.<sup>[6b,22]</sup> Generally, the addition of trivalent elements can enhance the formation of oxygen vacancies by replacing two  $\text{Ce}^{4+}$  ions with two trivalent cations in the ceria lattice. Reddy et al.<sup>[23]</sup> prepared  $\text{Zr}^{4+}$ - and  $\text{Al}^{3+}$ -doped  $\text{CeO}_2$  nanocatalysts by a wet impregnation method, and Mao et al.<sup>[24]</sup> synthesized nitrogen-doped ceria NPs by a wet-chemical route. It has been reported that calcia-doped ceria with amorphous silica synthesized by using a seeded polymerization technique has excellent UV-light absorption properties and shows higher catalytic performance for the oxidation of organic materials than undoped ceria.<sup>[25]</sup> Dense  $\text{Ce}_{0.8}\text{Pr}_{0.2}\text{O}_{2-\delta}$  ceramic membranes with micrometer grain sizes can be synthesized at 1000 °C by minor doping of cobalt oxide and behave with higher levels of oxygen permeability.<sup>[26]</sup> Particularly,  $\text{CeO}_2$  can act as an oxygen buffer by releasing/restoring oxygen through redox processes involving the  $\text{Ce}^{4+}/\text{Ce}^{3+}$  couple, which plays an important role in many oxidation reactions. Recently, various ZnO nanostructures with tunable optoelectronic properties, such as tetrapods and

Dr. X.-H. Guo, Prof. W.-X. Huang, Prof. S.-H. Yu  
Division of Nanomaterials & Chemistry  
Hefei National Laboratory for  
Physical Sciences at Microscale  
Department of Chemistry  
Department of Chemical Physics  
National Synchrotron Radiation Laboratory  
University of Science and Technology of China  
Hefei 230026, P.R. China  
E-mail: shyu@ustc.edu.cn



Dr. X.-H. Guo, Dr. C.-C. Mao, J. Zhang, W.-N. Wang, Prof. Y.-Y. Wang  
Key Lab of Synthetic and Natural Functional  
Molecule Chemistry of Ministry of Education, and  
the College of Chemistry and Materials Science  
Northwest University  
Xi'an 710069, P.R. China  
E-mail: guoxh2009@nwu.edu.cn

Dr. J. Huang, Dr. Y.-H. Deng, Prof. Y. Cao  
Department of Chemistry  
Fudan University  
Shanghai 230024, P.R. China

DOI: 10.1002/sml.201102179

ultrathin nanowires,<sup>[27]</sup> have been synthesized by simply varying the Mg dopant amount in the range from 0 to 50 at.%. Thus, desirable doping could improve the properties and control the morphologies of many metal oxide nanostructures.

Although doped ceria systems have been extensively investigated in the literature, the influence of doping in ceria NPs with various low-dimensional nanostructures at a wide range of doping levels (even higher than 20–25 at.%) has not been systematically investigated.<sup>[28]</sup> 2D ceria nanostructures have stimulated enormous interest because of their novel properties associated with morphology or surface structure and their significant promise as building blocks for functional materials, devices, and systems.<sup>[20,29]</sup>

Herein, we report a facile synthesis of unique ceria nanostructures with triangular column, triangular slab, and disklike shapes by simply tuning the cobalt nitrate doping levels under mild hydrothermal conditions. Particularly, the prepared ceria nanostructures can be used as desired low-temperature catalysts for CO oxidation, and show significantly enhanced catalytic activity and higher stability than commercial ceria powder. A systematic investigation of the cobalt doping effect on the catalytic activity of the prepared ceria samples through morphological and structural variation will be reported.

Ceria samples with different morphologies can be prepared by adjusting the doping level of cobalt nitrate in solution under hydrothermal conditions at 160 °C for 24 h, followed by calcination at 550 °C for 6 h (**Figure 1**, and Supporting Information Figure S1). When doped with 2 wt.% cobalt nitrate, a kind of irregular triangular columnlike ceria particle is obtained (Figure 1a), which displays an obviously layered feature.

If the doping amount of cobalt nitrate was increased to 5 wt.%, triangular slablike ceria particles with porous features on their surfaces could be obtained (Figure 1b); the average thickness of the slablike particle was  $\approx 260$  nm. Interestingly, when the doping amount of cobalt nitrate was further increased to 10 wt.%, incomplete disklike structures were

observed (Figure 1c). The obtained sample was composed of incomplete disklike particles and a small number of irregular epitaxial patches, and the mean thickness and diameter of the disklike ceria particles were  $\approx 75$  nm and 1.15  $\mu\text{m}$ , respectively. When the doping amount was increased to 20 wt.%, well-defined and high-quality disklike nanostructures were obtained (Figure 1e), and the nanodisks displayed very smooth surface features and their mean thickness was  $\approx 70$  nm (Figure 1e). However, if no cobalt source was added, only irregular layered triangle-like ceria structures with a broader size distribution were obtained (see Supporting Information Figure S2). In contrast, pure  $\text{Co}_3\text{O}_4$  product could be prepared when no cerium source was introduced (Figure 1f and Supporting Information Figure S3). The as-obtained  $\text{Co}_3\text{O}_4$  exhibited typically porous and bulk cubelike features.

After calcination at 550 °C for 6 h, the ceria-based precursors prepared by a hydrothermal process at 160 °C for 24 h show no change in morphology (see Supporting Information Figure S1). The prepared ceria precursor before calcination can be readily indexed to the pure orthorhombic phase of cerium hydroxide carbonate (JCPDS card no. 52-0352; see Supporting Information Figure S4). In addition, all the obtained ceria samples after calcination can be indexed to pure fluorite-like cubic-phase ceria (see Supporting Information Figure S5), and thus no diffraction peaks of  $\text{Co}_3\text{O}_4$  were observed even when the cobalt nitrate doping amount was up to 20 wt.%, which implied that elemental Co was highly distributed in the ceria sample rather than incorporated into the ceria lattice. Therefore, it can be inferred that 2D disklike ceria nanostructures can be easily tailored by altering the doping amount of cobalt nitrate.

Uniform and porous disklike ceria can be clearly observed in the transmission electron microscopy (TEM) image in **Figure 2a**. The high-resolution TEM (HRTEM) image in Figure 2b of a typical disklike ceria particle shows well-defined crystal lattice stripes, and the spacings are measured to be 3.02 and 1.82 Å, corresponding to {111} and

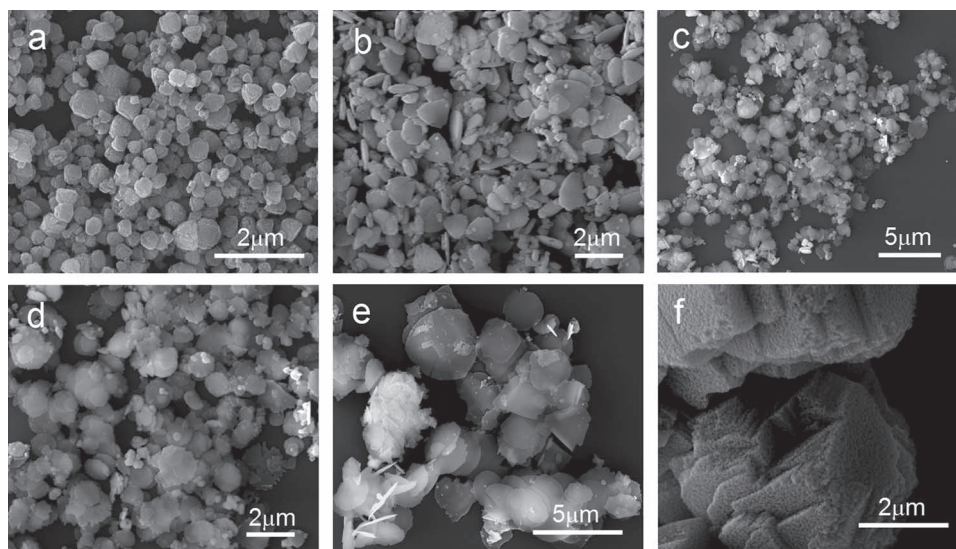


**Figure 1.** Scanning electron microscopy (SEM) images of ceria particles prepared by changing the doping amount of cobalt nitrate: a) 2, b) 5, c, d) 10, e) 20, and f) 100 wt.%. The samples were prepared by hydrothermal reaction at 160 °C for 24 h, followed by calcination at 550 °C for 6 h.

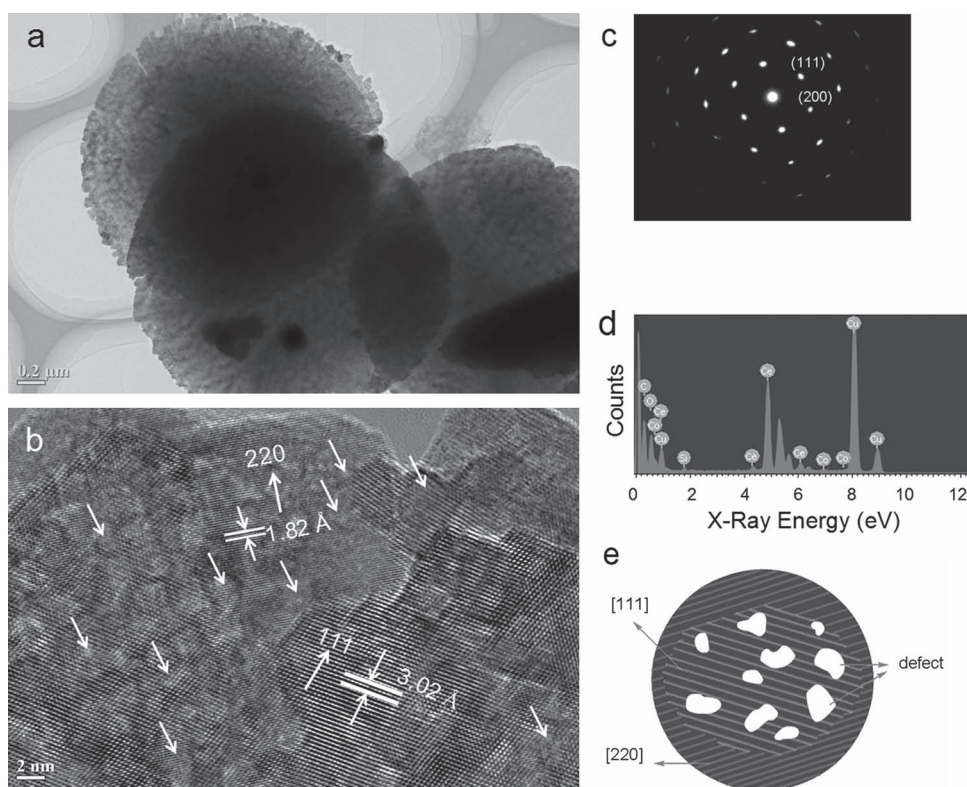


**Figure 2.** Structural analysis of typical porous ceria nanodisks formed by doping with 20 wt.% cobalt nitrate. a) TEM image; b) HRTEM image of nanodisks (arrows represent dislocations); c) SAED pattern; d) EDS of the ceria nanodisk; e) schematic illustration of a ceria particle with obvious surface defects on the crystal surface.

{220} planes, respectively, which agree well with the X-ray diffraction (XRD) pattern and selected-area electron diffraction (SAED) results (Figure 2c). In addition, the presence of Co, Ce, and O elements in the energy-dispersive spectroscopy (EDS) results further confirms the validity of the obtained cobalt-doped ceria sample (Figure 2d). In particular, some dislocations or grain boundaries among the crystal lattices were observed in Figure 2b, which are visually depicted by the white micro-areas located in Figure 2e.

On the other hand, we investigated the formation process of such unique ceria nanodisks, which show obvious advantages in catalytic performance for CO oxidation. Time-dependent experiments were performed to investigate the formation process of the disks (see Supporting Information Figure S6). The ceria NPs formed at an early stage can undergo a transformation from spherical to thicker slabs, and finally to nanodisks as the reaction proceeds. After 2 h of reaction, the obtained ceria particles were spherical in shape and polycrystalline (see Supporting Information Figure S7). When the reaction was prolonged to 4 h, a kind of uniform and porous slablike intermediate was formed (see Supporting Information Figure S8). Interestingly, imperfect nanodisklike structures can be obtained when the reaction time is up to 8 h, and the particles are single-crystalline (see Supporting Information Figure S9), but distinct grain boundaries can be clearly observed. Similarly, directed growth of ZnO and WO<sub>3</sub> nanodisks exploits this adsorption of molecules to certain crystal facets with great success.<sup>[30]</sup> In addition, ceria nanosheets can be formed through 2D self-organization of initially formed

small ceria nanocrystals and a subsequent recrystallization process.<sup>[20]</sup> Xiao et al. reported that layered Sm<sub>2</sub>O<sub>3</sub> nanodisks could be obtained by a nonaqueous sol-gel process, by considering that the initially formed irregular aggregates at an early reaction stage tended to grow into spherical aggregates, and then further self-assembled into individual porous nanodisks through an oriented attachment process.<sup>[31]</sup> Based on these observations, we propose that the formation of ceria nanodisks is mainly driven by the preferential adsorption of cetyltrimethylammonium bromide (CTAB) onto the (110) crystal facets and inhibition of its crystallographic growth, and it further undergoes the oriented attachment process along {220} planes and fusion of primary spherical NPs.

The chemical states of the Ce and O species on the catalyst surface were investigated by X-ray photoelectron spectroscopy (XPS; see Supporting Information Figure S10). The main O 1s peak at around 529 eV was assigned to lattice oxygen of CeO<sub>2</sub> (see Supporting Information Figure S10a). A higher binding energy shoulder was observed for all samples at about 531 eV, which can be assigned to a mixture of surface hydroxyl and carbonate groups. The Ce 3d XPS spectra exhibit multiple states arising from different Ce 4f level occupancies in the final state (see Supporting Information Figure S10b, wherein *V* and *U* refer to the 3d<sub>5/2</sub> and 3d<sub>3/2</sub> spin-orbital components, respectively). The Ce<sup>III</sup>/Ce<sup>IV</sup> atomic ratio in various catalysts that indicates the concentration of surface oxygen vacancies was also calculated by the peak area of Ce<sup>III</sup>/the total area of Ce<sup>IV</sup> peaks. Additionally, the Co 2p peak at around 825 eV was observed (see Supporting Information Figure 10c), which

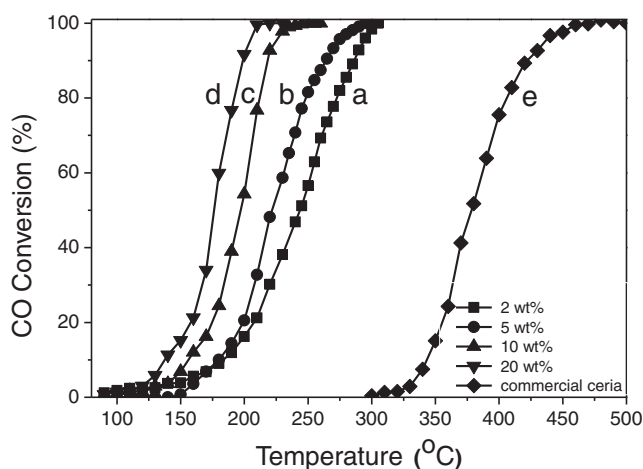


**Figure 3.** Catalytic activity of CO oxidation over different ceria catalysts prepared by varying the cobalt nitrate doping level by hydrothermal reaction at 160 °C for 24 h, followed by calcination at 550 °C for 6 h: a) 2, b) 5, c) 10, d) 20 wt.%, and e) commercial ceria powder.

implies that the elemental Co was completely doped into the ceria sample. Additional information on the surface electronic states of different ceria samples can also be obtained from UV/Vis diffuse reflectance measurement (see Supporting Information Figure S11A). The bandgap of the obtained ceria can be estimated. The bandgaps of the ceria samples prepared with cobalt nitrate doping amounts of 2, 5, 10, and 20 wt.% are 2.55, 2.47, 2.29, and 2.37 eV, respectively (see Supporting Information Figure S11B). Raman spectroscopy was used to determine the exact phase or crystal structure of the cobalt-doped ceria samples (see Supporting Information Figure S12). The presence of the characteristic peak at  $\approx 461\text{ cm}^{-1}$  for the fluorite ceria structure is observed (see Supporting Information Figure S12), which is in good agreement with that of a previous report.<sup>[32]</sup>

The catalytic performances of the cobalt-doped  $\text{CeO}_2$  catalysts in CO oxidation are shown in **Figure 3**. It is clearly found that ceria nanodisks are more active than the other three ceria samples, as well as commercial ceria powder. At 171 °C, the percentage of CO conversion is 40% over  $\text{CeO}_2$  nanodisks but only 18 and 7% for imperfect nanodisk and triangular slablike particles, respectively. The reaction temperature for 100% CO conversion over the disklike ceria particles is measured to be  $\approx 210\text{ °C}$ , which is much lower than that of previous reports.<sup>[16,32,33]</sup> In addition, the catalytic activity for the Co-doped ceria increases with the increasing of cobalt doping level, corresponding to the decrease of the bandgap. Also, the light-off temperature  $T_{50}$ , corresponding to 50% conversion of CO, is shown in **Table 1**. All of these data demonstrate that the  $\text{CeO}_2$  nanodisk is more active than the reported ceria nanostructures.

For comparison, the activities of the parent ceria are also included in Figure 3 and Table 1. It is clear that the activities of Au-containing catalysts are remarkably higher than those of the corresponding parent ceria support materials (see Supporting Information Figure S13). The temperature at which the conversion was 50% ( $T_{1/2}$ ) for ceria nanodisks is 449 K, which is 175 K higher than that for Au–ceria nanodisk catalyst,

**Table 1.** Summary of crystal structural parameters, pore features, and CO conversion over ceria catalysts prepared by varying the doping amount of cobalt nitrate.

Sample	Doping amount [wt.%]	Cell parameter [Å]	$D^b$ [nm]	$S_{\text{BET}}^c$ [ $\text{m}^2\text{ g}^{-1}$ ]	$T_{50}$ [°C]
1 <sup>a)</sup>	0	5.4112			374
2	2	5.4083	2.15	50.0	243
3	5	5.4082	2.16	49.3	221
4	10	5.4080	6 + 66.8 <sup>d)</sup>	37.2	196
5	20	5.3972	8.1	31.6	176

<sup>a)</sup>Sample 1 represents commercial ceria; <sup>b)</sup> $D$  represents pore diameter; <sup>c)</sup> $S_{\text{BET}}$  represents specific surface area. The crystal cell parameter was calculated based on MDI Jade software.

<sup>d)</sup>Sample 4 possesses two sets of pore size distributions, 6 and 66.8 nm.

thus showing its enhanced low-temperature catalytic activity for CO oxidation. Moreover, the catalytic activity of the Au-loaded ceria nanodisks can be kept without loss throughout the oxidation reaction process performed at 25 °C for 18 h (see Supporting Information Figure S14), thus implying their remarkable catalytic stability. Based on the above results, it was found that the surface microstructure of the  $\text{CeO}_2$ -nanodisk support displayed advantages by avoiding diffusion or mass-transfer limitation.

It is well known that catalytic nanomaterials with high specific surface area, and numerous crystal facets, edges, and corners, which are conventionally considered as active sites for the adsorption of reactants,<sup>[34]</sup> should display better catalytic performance. Nevertheless, among the present  $\text{CeO}_2$  nanostructures, ceria nanodisks with lower surface area and larger diameter are especially more active and possess stable redox properties. As a result, these unusual results for novel ceria nanostructures inspired us to explore the key factors that are responsible for the enhanced CO oxidation activity.

It is reported that the formation energy of anion vacancies for different  $\text{CeO}_2$  surfaces follows the order  $\{110\} < \{100\} < \{111\}$  according to theoretical molecular calculations.<sup>[33]</sup> Therefore, since less energy is required to form an oxygen vacancy on these surfaces, it can facilitate accommodation and sequentially involve reaction with CO,<sup>[33]</sup> which implies that many more  $\text{Ce}^{3+}$  components can be produced and stabilized around the oxygen vacancies on the surface of ceria. Herein, when doping with 2 wt.% cobalt nitrate, the obtained ceria particles always expose highly stable  $\{111\}$  planes (see Supporting Information Figure S15). At the same time, the obtained ceria particles in the case of doping with 5 wt.% cobalt nitrate finally expose  $\{111\}$  planes (see Supporting Information Figure S16). However, if the cobalt nitrate doping amount was increased to 10 wt.%, the prepared ceria sample always exposed mostly  $\{111\}$  planes and a small fraction of  $\{200\}$  planes (see Supporting Information Figure S17). Notably, it was easily observed that the exposed planes of the obtained ceria nanodisks in the case of doping with 20 wt.% cobalt nitrate are  $\{200\}$  planes in the majority of cases and some of them are  $\{111\}$  planes (Figure 2b), since the  $\{200\}$  planes can significantly increase the oxygen diffusion rates and the ease of formation of many more oxygen vacancies on the surface of ceria.<sup>[35]</sup> As a result, the ceria nanodisks are

more active than other cobalt-doped ceria samples in the CO oxidation.

Additionally, we also investigated the shape effect of single-crystalline CeO<sub>2</sub> on the redox behavior of a series of hydrothermally derived CeO<sub>2</sub> materials. Yan et al.<sup>[32]</sup> disclosed that the CeO<sub>2</sub> nanorod is much more active for CO oxidation than CeO<sub>2</sub> nanopolyhedra. Li et al.<sup>[33a]</sup> demonstrated that CeO<sub>2</sub> nanorods with preferable {001} exposure planes exhibit enhanced redox properties for CO oxidation compared to normal ceria materials. This can facilitate the migration of oxygen vacancies from the bulk to the ceria surface. Our results confirm that, by exposing more reactive surfaces or oxygen vacancies of the crystalline ceria nanodisks, it is feasible to design new improved ceria-based catalysts with enhanced redox properties.

On the other hand, the prepared nanostructured ceria samples after the CO catalytic oxidation reaction can be indexed to a mixture of the rhombohedral phase of Ce<sub>7</sub>O<sub>12</sub> and a trace amount of fluorite cubic ceria (see Supporting Information Figure S18), which means that most Ce<sup>4+</sup> ions have been changed into Ce<sup>3+</sup> through oxygen redox reaction, namely, many more oxygen vacancies can be formed on the surface of ceria. That is indeed essential for CO catalytic oxidation. Moreover, if the ceria support can be loaded with Au NPs to form Au–ceria catalyst, then the Au–ceria catalyst after CO oxidation can be indexed to an almost rhombohedral phase of Ce<sub>7</sub>O<sub>12</sub> (see Supporting Information Figure S19), which can directly verify that the Ce<sup>4+</sup> has been completely changed into Ce<sup>3+</sup> in the presence of Au NPs. Consequently, we can infer that almost all the Ce<sup>4+</sup> ions can take part in the O<sup>•</sup> formation process in this case. This can well explain why the low-temperature catalytic activity of nanodisklike ceria loaded with Au NPs behaves much better than pure nanodisk ceria.

To address the role of surface defect effects in mediating the catalytic activity for CO oxidation, electron paramagnetic

resonance (EPR) spectra were obtained for the nanodisk ceria sample formed by doping with 20 wt.% cobalt nitrate before and after the CO oxidation reaction (**Figure 4**). The strongest signal peak is observed due to the typical characteristic of Ce<sup>3+</sup> ions containing unpaired electrons.<sup>[36]</sup> The observed variation in the EPR signal intensity corresponding to Ce<sup>3+</sup>–O–Ce<sup>4+</sup>-type defect sites was recorded for ceria nanodisks before and after CO catalytic oxidation occurred. It was found that the EPR signal intensity  $g_{\perp}$  was 1.96 before catalytic reaction, which corresponded to the surface Ce<sup>3+</sup> concentration, wherein the number of Ce<sup>3+</sup> ions obtained from integrating the EPR spectra can reflect the real concentration of oxygen vacancies.<sup>[37]</sup> This case can also be evidenced from Figure 2b. However, the EPR signal intensity almost disappears after the CO catalytic oxidation reaction is complete (Figure 4b). This result demonstrates that the Ce<sup>3+</sup> defect site concentration on the surface of the ceria sample can significantly exert a redox ability over the CO oxidation. The presence of defects can result in the generation of microstrain in the ceria crystal lattice. From the XRD patterns and Table 1, although we can see that the triangular slablike ceria particles possess the highest lattice strain compared with the other three samples, the imperfect nanodisks follow, and their catalytic activity is not the highest, which means that the enhanced catalytic activity for ceria is mainly dominated by the exposed highly active {220} planes rather than lattice distortion effects.

In summary, we have reported a facile synthesis recipe for the preparation of high-quality CeO<sub>2</sub> nanodisks by controlling the doping amount of cobalt nitrate in a hydrothermal reaction. The CeO<sub>2</sub> nanodisks show not only excellent catalytic activity but also enhanced catalytic stability. Compared with commercial ceria powder, these cobalt-doped CeO<sub>2</sub> nanostructures behave with the characteristics of uniform 2D disklike nanostructures, with exposed {220} planes as well as a large number of oxygen vacancies on the surface of the ceria, which are responsible for the improved catalytic activity in CO oxidation. The presented synthesis approach can be applied to the synthesis of other rare-earth nanostructures with specific morphology and textures. Furthermore, this finding will open a new avenue for the preparation of transition-metal-doped ceria with improved catalytic activity, and may serve as an excellent model of both theoretical and practical interest in high-temperature catalytic systems.

## Experimental Section

**Chemicals:** Ce(NO<sub>3</sub>)<sub>3</sub>·6H<sub>2</sub>O (Beijing Chem. Corp., China) was used as the cerium source. Cobalt nitrate (Co(NO<sub>3</sub>)<sub>2</sub>·6H<sub>2</sub>O, Shanghai Chem. Corp., China) was used as cobalt dopant source. Cetyltrimethylammonium bromide (CTAB; Aldrich) and ethanol (C<sub>2</sub>H<sub>6</sub>O, >99.7%) were used as received.

**Synthesis of the Ceria Samples:** In a typical synthesis, 0.85 g Ce(NO<sub>3</sub>)<sub>3</sub>·6H<sub>2</sub>O and different amounts of cobalt nitrate (0.012–0.14 g) were dissolved in deionized water (40 mL). Then, CTAB (0.25 g) was added to the solution and magnetic stirring was continued. After that, urea (4.80 g) was added to the obtained solution to form a milky solution. The resultant homogeneous solution

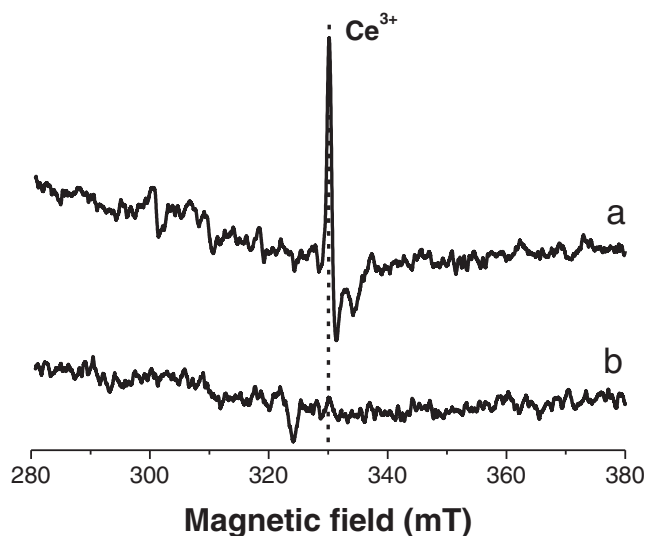


**Figure 4.** Representative EPR spectra of the ceria sample prepared by doping with 20 wt.% cobalt nitrate via hydrothermal treatment at 160 °C for 24 h, followed by calcination at 550 °C for 6 h: a) before catalytic reaction; b) after catalytic reaction. All EPR measurements were performed at room temperature.

was dispersed in a Teflon-lined autoclave with a volume of 80 mL for different reaction times at 160 °C, and then the autoclave was cooled to room temperature. The obtained light-yellow precipitates were separated by centrifugation, washed with deionized water and ethanol several times, and dried at 60 °C in air overnight. Finally, the obtained yellow powders were calcined at 550 °C for 6 h at a heating rate of 2 °C min<sup>-1</sup> to obtain white-brown ceria samples.

**Preparation of Au–CeO<sub>2</sub> Catalyst:** The deposition of Au NPs onto the ceria nanodisks was performed by using a routine deposition–precipitation method originally developed by Haruta et al.<sup>[38]</sup> Briefly, the CeO<sub>2</sub> substrates were dispersed in an aqueous solution of HAuCl<sub>4</sub> at a fixed pH of 10. The nominal Au loading was 3.0 wt.%. The suspension was aged at 333 K for 2 h and washed with deionized water several times. The final Au-containing ceria material was obtained by calcination in air at 523 K for 2 h.

## Supporting Information

Supporting Information is available from the Wiley Online Library or from the author. It includes results from characterization, SEM, XRD, TEM, HRTEM, EDS, XPS, Raman spectroscopy, UV/Vis spectroscopy, and the CO catalytic oxidation tests.

## Acknowledgements

We acknowledge the funding support from the National Basic Research Program of China (2010CB934700), the National Science Foundation of China (Nos. 21001087, 21073040, 21173167, 91022032, 21061160492, J1030412), the Principal Investigator Award by the National Synchrotron Radiation Laboratory at USTC, the Education Committee of Shanxi Province (Grant Nos. 2010JK870, 2010JS115), and the open project of inorganic synthesis and preparation chemistry, National Key Lab of Jinlin University (No. 2012-09).

- [1] a) I. Lisiński, *J. Phys. Chem. B* **2005**, *109*, 122310; b) G. R. Partzke, F. Krumerich, R. Nesper, *Angew. Chem.* **2002**, *114*, 2554; *Angew. Chem. Int. Ed.* **2002**, *41*, 2446.
- [2] S. Sun, C. B. Murray, D. Weller, L. Folks, A. Moser, *Science* **2000**, *287*, 1989.
- [3] a) S. J. Park, S. Kim, S. Lee, Z. G. Khim, K. Char, T. Hyeon, *J. Am. Chem. Soc.* **2000**, *122*, 8581; b) J. W. Stouwdam, F. C. J. M. Veggel, *Nano Lett.* **2002**, *2*, 733; c) F. Dumestre, B. Chaudret, C. Amienes, M. C. Fromen, M. J. Casanove, P. Renaud, P. Zurcher, *Angew. Chem.* **2002**, *114*, 4462; *Angew. Chem. Int. Ed.* **2002**, *41*, 4286.
- [4] Z. G. Yan, C. H. Yan, *J. Mater. Chem.* **2008**, *18*, 5046.
- [5] S. W. Boettcher, J. Fan, C. K. Tsung, Q. H. Shi, G. D. Stucky, *Acc. Chem. Res.* **2007**, *40*, 784.
- [6] a) Y. S. Chaudhary, S. Panirahi, S. Nayak, B. Satpanti, S. Bhattacharjee, N. Kulkarni, *J. Mater. Chem.* **2010**, *20*, 2381; b) A. Corma, P. Atienzar, H. Garcia, J. Y. Chane-Ching, *Nat. Mater.* **2004**, *3*, 394.
- [7] a) R. Cui, W. C. Lu, L. M. Zhang, B. H. Yue, S. Shen, *J. Phys. Chem. C* **2009**, *113*, 21520; b) A. Asati, S. Santra, C. Kaittanis, S. Nath, J. M. Perez, *Angew. Chem.* **2009**, *121*, 2344; *Angew. Chem. Int. Ed.* **2009**, *48*, 2308.
- [8] Y. Ma, X. D. Wang, S. H. Li, M. S. Toprak, B. Zhu, M. Muhammed, *Adv. Mater.* **2010**, *22*, 1640.
- [9] L. He, J. Ni, L. C. Wang, F. J. Yu, Y. Cao, H. Y. He, K. N. Fan, *Chem. Eur. J.* **2009**, *15*, 11833.
- [10] R. Si, Y. W. Zhang, L. P. You, C. H. Yan, *Angew. Chem.* **2005**, *117*, 3320; *Angew. Chem. Int. Ed.* **2005**, *44*, 3256.
- [11] J. Liu, Z. Zhao, J. Q. Wang, C. M. Xu, A. J. Duan, G. Y. Jiang, Q. Yang, *Appl. Catal. B* **2008**, *84*, 185.
- [12] W. S. Jung, H. S. Park, Y. J. Kang, D. H. Yoon, *Ceram. Int.* **2010**, *36*, 371.
- [13] B. Aiken, W. P. Hsu, E. Matijevic, *J. Am. Ceram. Soc.* **1988**, *71*, 845.
- [14] D. J. Chen, R. Ran, K. Zhang, J. Wang, Z. P. Shao, *J. Power Sources* **2009**, *188*, 96.
- [15] C. S. Pan, D. S. Zhang, L. Y. Shi, *J. Solid State Chem.* **2008**, *181*, 1298.
- [16] H. P. Zhou, Y. W. Zhang, S. Rui, L. S. Zhang, W. G. Song, C. H. Yan, *J. Phys. Chem. C* **2008**, *112*, 20366.
- [17] M. Inoue, M. Kimura, T. Inui, *Chem. Commun.* **1999**, 957.
- [18] J. Zhang, S. Ohara, M. Umetsu, Y. Hatakeyama, T. Adschiri, *Adv. Mater.* **2007**, *19*, 203.
- [19] T. Yu, J. Joo, Y. I. Park, T. Hyeon, *Angew. Chem.* **2005**, *117*, 7577; *Angew. Chem. Int. Ed.* **2005**, *44*, 7411.
- [20] T. Yu, B. Lim, Y. N. Xia, *Angew. Chem.* **2010**, *122*, 4586; *Angew. Chem. Int. Ed.* **2010**, *49*, 4484.
- [21] S. Babu, R. Thanneeru, T. Inerbaer, R. Day, A. E. Masunov, A. Schulte, S. Seal, *Nanotechnology* **2009**, *20*, 085713.
- [22] a) R. O. Fuentes, F. Munoz, L. M. Acuna, A. G. Leyva, R. T. Baker, *J. Mater. Chem.* **2008**, *18*, 5689; b) J. Hugo, A. Paredes, K. Choi, C. T. Chen, S. Kim, *J. Mater. Chem.* **2009**, *19*, 4837.
- [23] B. M. Reddy, K. N. Rao, G. K. Reddy, *Catal. Lett.* **2009**, *131*, 328.
- [24] C. J. Mao, Y. X. Zhao, X. F. Qiu, J. J. Zhu, C. Burda, *Phys. Chem. Chem. Phys.* **2008**, *10*, 5633.
- [25] A. M. El-Toni, S. Yin, Y. Hayasaka, T. Sato, *J. Mater. Chem.* **2005**, *15*, 1293.
- [26] D. P. Fagg, S. Garcia-Martin, V. V. Kharton, J. R. Frade, *Chem. Mater.* **2009**, *21*, 381.
- [27] Y. Yang, Y. Z. Jin, H. P. He, Q. L. Wang, Y. Tu, H. M. Lu, Z. Ye, *J. Am. Chem. Soc.* **2010**, *132*, 13381.
- [28] P. J. Gellings, H. J. M. Bouwmeester, *Catal. Today* **2000**, *58*, 1.
- [29] M. Choi, K. Na, J. Kim, Y. Sakamoto, O. Terasaki, R. Ryoo, *Nature* **2009**, *461*, 246.
- [30] a) A. Wolcott, T. R. Kuykendall, W. Chen, S. W. Chen, J. Z. Zhang, *J. Phys. Chem. B* **2006**, *110*, 25288; b) C. Kim, Y. J. Kim, E. S. Jang, G. C. Yi, H. Kim, *Appl. Phys. Lett.* **2006**, *88*, 093104.
- [31] H. Y. Xiao, P. N. Li, F. L. Jia, L. Z. Zhang, *J. Phys. Chem. C* **2009**, *113*, 21034.
- [32] R. Si, Y. W. Zhang, S. J. Li, B. X. Lin, C. H. Yan, *J. Phys. Chem. B* **2004**, *108*, 12481.
- [33] a) K. B. Zhou, X. Wang, X. M. Sun, Q. Peng, Y. D. Li, *J. Catal.* **2005**, *229*, 206; b) X. S. Huang, H. Sun, L. C. Wang, Y. M. Liu, K. N. Fan, Y. Cao, *Appl. Catal. B* **2009**, *90*, 224.
- [34] D. Terribile, A. Trovarelli, C. de Leitenburg, G. Dolcetti, *Chem. Mater.* **1997**, *9*, 2676.
- [35] R. Si, M. F. Stephanopoulos, *Angew. Chem.* **2008**, *120*, 2926; *Angew. Chem. Int. Ed.* **2008**, *47*, 2884.
- [36] B. Murugan, A. V. Ramaswamy, *J. Am. Chem. Soc.* **2007**, *129*, 3062.
- [37] M. W. Zhao, M. Q. Shen, J. Wang, *J. Catal.* **2007**, *48*, 258.
- [38] M. Haruta, S. Tsubota, T. Kobayashi, H. Kageyama, M. J. Genet, B. Delmon, *J. Catal.* **1993**, *144*, 175.

Received: October 15, 2011  
 Revised: December 12, 2011  
 Published online: March 13, 2012